To access the final edited and published work see
https://doi.org/10.1109/LAWP.2025.3557192

Adaptive On-the-fly Scan Method for Fast and Efficient Planar Near-field Acquisition

Cheng Yang, *Senior Member, IEEE,* Tomas Monopoli, Sebastian Götschel, Xinglong Wu, *Senior Member, IEEE,* Flavia Grassi, *Senior Member, IEEE,* and Christian Schuster, *Fellow, IEEE*

***Abstract*—Recent advancements in adaptive planar near-field scanning have enhanced the use of sparse measurement data for electromagnetic field (EMF) modeling and prediction. In this work, we propose an adaptive planar scanning solution that utilizes iterative row-by-row scans, where each row is scanned on-the-fly (OTF). Both the total number of rows and their separation are dynamically adjusted and optimized through correlation analysis of the values obtained from previous measurements. For initialization, a few evenly distributed row scans, typically 4-6 OTF scans, are performed, followed by an iterative process of finding new rows to scan using Gaussian Process Regression (GPR) based Bayesian optimization. For validation, both numerical and experimental examples, including wire and patch antenna arrays, are provided. Results show good performance of the proposed method, enabling rapid near-field acquisition within minutes, making it suitable for large-scale and high-resolution EMF scanning applications.**

***Index Terms*—Near-field measurement, adaptive sampling, on-the-fly scan, Bayesian optimization, Gaussian Process.**

I. Introduction

RADIO frequency near-field scan (NFS) measurement is a sophisticated technique with wide-ranging applications, such as integrated circuits, antenna measurements, and electromagnetic compatibility (EMC) tests [1], [2]. Due to variations of field distribution at sub-wavelength scale, near-field scanning generally requires much higher spatial resolution compared to far-field measurements. Depending on the field probe in-use and the performance of the positioning system, the best spatial resolution achievable in near-field scanning typically begins at several tens of micrometers. Hence, when performing an equidistant near-field scan with sub-millimeter spatial resolution, even a scan area of just a few centimeters can require significant time and effort.

Over the past decade, researchers and engineers have made extensive efforts to provide effective solutions, reducing both the required sampling points and the average measurement time per point. For example, the total number of points required for NFS, can been minimized through adaptive field acquisition using sparse sampling techniques. These include iterative sampling using interpolation technique [3]–[5], machine learning (ML) method [6], [7], and sequential spatial adaptive sampling [8], [9]. These approaches have shown successful applications in benchmark examples with experiments. Meanwhile, high-bandwidth instruments and high-speed scanning gantries have been integrated in modern NFS systems, greatly reducing measurement times and waiting periods. This enables NFS in motion, known as on-the-fly (OTF) scanning, drift scanning, or raster scanning [10], as an alternative method to minimize scanning time.

Recently, the OTF method has been further enhanced based on a new reformulation of the problem from a signal processing perspective [11]–[13], eliminating overall communication overhead during the measurement which will be briefly described in Sec. II. Building on this new OTF scan technique, we propose a novel adaptive scanning method for planar NFS that utilizes iterative OTF scans rather than traditional point-wise scans. The remainder of this paper will first explain the details of this approach, followed by numerical and experimental validations, and final a conclusion.

II. Adaptive OTF Scan Approach

As shown in Fig. 1, the OTF scan begins with a predefined motion profile, $y(t)$, which specifies the full scanning time and velocity. During the scan, the transient probe signal is fully captured as $u(t)$. Theoretic derivation discloses that the motion effects on the induced probe signal corresponds to a magnitude- and phase-modulation. Through in-phase and quadrature (IQ) demodulation followed by time-to-space mapping, the spatial complex field distribution, $H(y)$ and $\phi(y)$, can be precisely reconstructed from $u(t)$ and $y(t)$. Notably, the enhanced OTF scan differs from the standard OTF scan in its continuous data acquisition and post-processing. A detailed formulation and explanation can be found in [11], [13]. In the following, the enhanced OTF scan method is to be applied to adaptive planar near-field scans.

In a planar near-field measurement, the traditional adaptive scan approach treats sampling as a 2D problem, using a step-scan method that captures the field point-by-point. By substituting a point-by-point scan with a line-by-line scan, we propose an adaptive OTF scan method. In this approach, iterative line scans are performed along the y-axis, from (x, y_a) to (x, y_b) at fixed x-coordinates, referred to as row

Manuscript received **, 2025; (Corresponding author: Cheng Yang.)

C. Yang and C. Schuster are with the Institut für Theoretische Elektrotechnik, Hamburg University of Technology (TUHH), 21079 Hamburg, Germany. (e-mail: cheng.yang@tuhh.de; schuster@tuhh.de)

S. Götschel is with the Chair Computational Mathematics, Institute of Mathematics, Hamburg University of Technology (TUHH), 21079 Hamburg, Germany. (e-mail: sebastian.goetschel@tuhh.de)

T. Monopoli, X. Wu, and F. Grassi are with the Department of Electronics, Information and Bioengineering, Politecnico di Milano, 20133 Milano, Italy. (e-mail: tomas.monopoli@polimi.it; xinglong.wu@polimi.it;flavia.grassi@polimi.it)

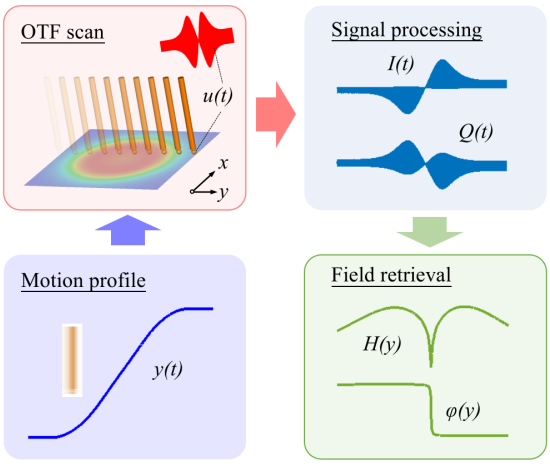

Fig. 1. Depiction of the enhanced OTF scan method with a coil antenna at a single frequency. The transient voltage signal, $u(t)$, from the fast-moving probe is fully captured, allowing millions of spatial samples per second along the scan path without sacrificing measurement accuracy [13].

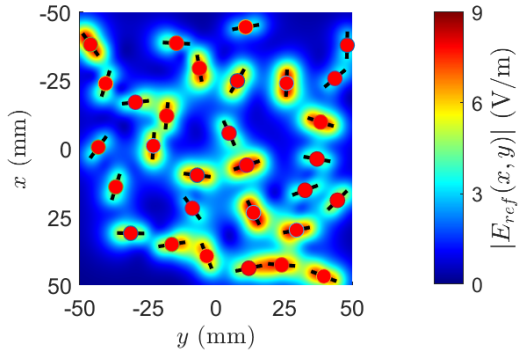

Fig. 2. Depiction of a nonuniform array consisting of 30 dipole wires, and the total E-field measured at $z = 5$ mm.

scans. Similarly, line scans can be conducted along the x-axis in the same manner. Each row scan leverages OTF to achieve a high-resolution field distribution, eliminating the need for resampling along the row dimension. As a result, regions with rapidly changing fields require more row scans than those with slowly varying fields, making the primary task of the adaptive OTF near-field acquisition the prediction of the optimal row for subsequent scanning. This can be achieved using a 1D Bayesian optimization (BO) approach, which is widely used to select the next evaluation sample based on prior observations.

Since the field values at a given row, comprising thousands of samples, are not suitable for BO, a statistical aggregate of the fields is used to create a 1D objective function, $G(x)$, representing all row scans and serving as the target for prediction. Here, the mean value is selected, and the objective function is defined as:

$$G(x) = \frac{1}{y_b - y_a} \int_{y_a}^{y_b} F(x, y')\, dy' \tag{1}$$

where $F(x, y)$ denotes the near-field data provided by a row scan at a given x. Next, surrogate modeling of $G(x)$ is performed using all prior row scans for building a probabilistic model in BO. As addressed in [5], [8], Gaussian Process Regression (GPR) can be used for surrogate modeling of $F(x, y)$. As a result, $G(x)$ also follows a Gaussian Process (GP) and its kernel function can be derived as:

$$k_G(x, x') = \frac{1}{(y_b - y_a)^2} \iint_{y_a}^{y_b} k_E((x, y), (x', y'))\, dy\, dy'. \tag{2}$$

where $k_E((x, y), (x', y'))$ stands for the kernel function of the GPR model of $F(x, y)$. Alternatively, $G(x)$ can be directly modeled using GPR, and a standard BO procedure [14] is then applied to $G(x)$ using a radial basis function kernel

$$k_{RBF}(x, x') = \exp\left(-\frac{|x - x'|^2}{2\ell^2}\right) \tag{3}$$

where ℓ is the scale length parameter. Finally, the next optimal row for next scanning is determined by using the upper confidence bound as the acquisition function

$$A(x) = \mu(x) + \kappa\sigma(x) \tag{4}$$

where $\mu(x)$ and $\sigma(x)$ are the GPR posterior mean and standard deviation at a given x, respectively. κ is a parameter that determines the exploration/exploitation balance: for high values of κ, the sampling tends to explore the whole parameter space; conversely, for low values of κ, the sampling tends to concentrate on regions of high field value. In this work, a value of $\kappa = 10$ was chosen to emphasize exploration. The sampling is interrupted when the surrogate models show no significant changes over multiple iterations, measured by correlation analysis with previous predictions.

III. Demonstration and Validation

To validate the approach, examples from both simulations and measurements, each featuring complex near-field distributions, are provided. The proposed method is used to obtain near-field results, which are then compared against high-resolution references to assess both efficiency and accuracy.

A. Wire Dipole Array

As illustrated in Fig. 2, an array of 30 short dipole wires is simulated using a Method of Moments (MoM) solver [15] at 100 MHz. The dipoles are randomly positioned within a 100 mm×100 mm area and are individually excited by complex voltage sources, with magnitudes ranging from 0.5 V to 1.5 V and phase angles from 0° to 90°. Each dipole is 10 mm in length and has a radius of 10 µm, ensuring a suitable aspect ratio for thin-wire assumptions. A high-resolution planar near-field acquisition, denoted as $E_{\text{ref}}(x, y)$, is conducted at a height of 5 mm above the dipole array, revealing a highly localized field distribution, as shown in Fig. 2. Following an initial scan of four equidistant rows along the y-axis, the adaptive OTF scan is iteratively conducted with a minimum of 20 row scans. Each row scan, performed at a specific x-coordinate, returns a 1D E-field distribution curve, as presented in Fig. 3(a).

Following (1), the target curve of averaged E-field distribution along x-axis is computed to predict the location for the

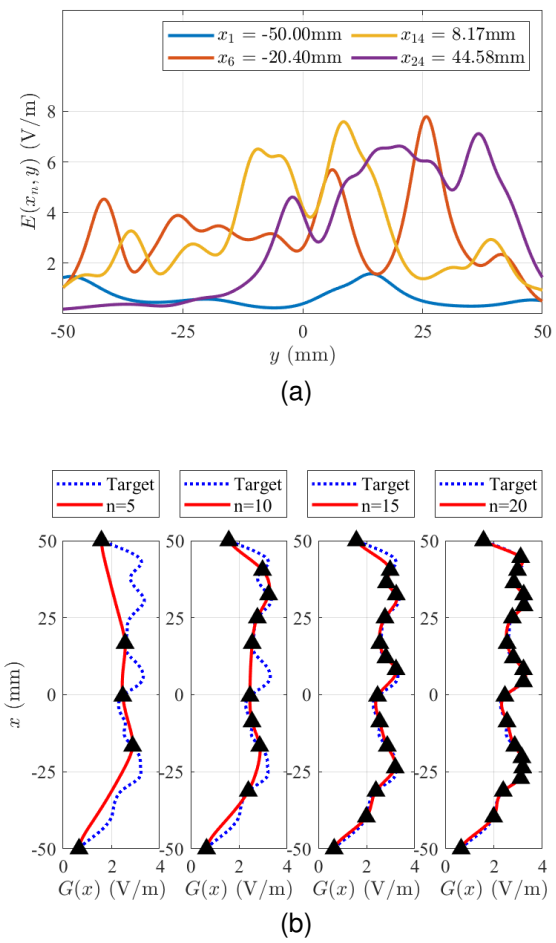

Fig. 3. Illustration of the adaptive OTF scan, showing (a) results of all row-wise scans, and (b) iterative predictions of $G(x)$ based on the first n scans.

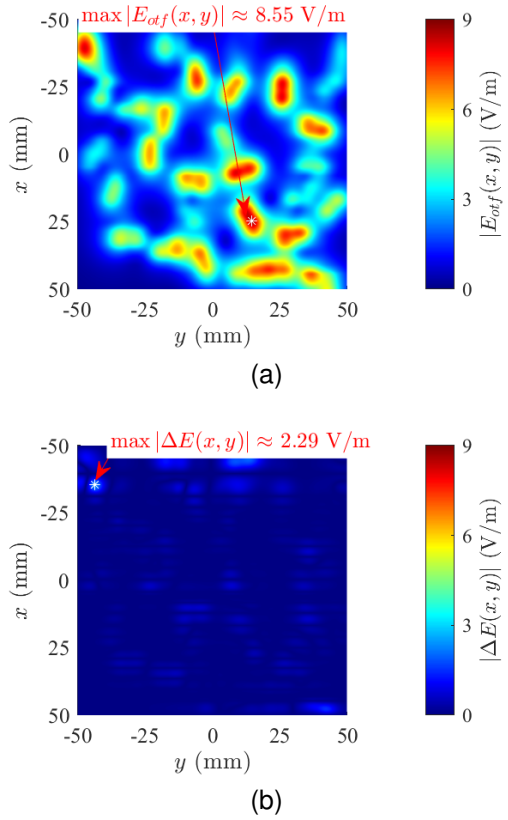

Fig. 4. Comparison of (a) E-field prediction obtained from adaptive OTF scan, and (b) its deviation to the reference E-field results provided in Fig. 2.

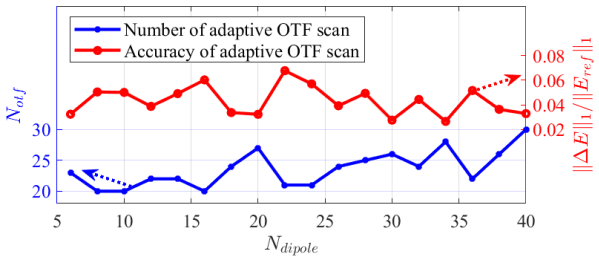

Fig. 5. Examination of the adaptive OTF scan by changing the number of dipole wires ranging from 5 to 40.

next row scan. The adaptive scanning process finishes once the convergence criterion is satisfied, as depicted in Fig. 3(b). Subsequently, the total E-field distribution is resampled over a dense grid using cubic interpolation, resulting in $E_{\text{otf}}(x, y)$, as shown in Fig. 4(a). For comparison, the E-field deviation is calculated as $\Delta E(x, y) = |E_{\text{otf}}(x, y) - E_{\text{ref}}(x, y)|$, which is illustrated in Fig. 4(b) and shows good agreement of the adaptive OTF scanning results with the reference ones. An additional performance analysis is performed by varying the dipole array size from 5 to 40 wires. The results of the parameter sweep are shown in Fig. 5. The analysis indicates that the impact of the dipole number on the required number of adaptive OTF scans, N_{otf}, remains limited, fluctuating between 20 and 30 in a non-monotonic manner. Measurement accuracy is evaluated by calculating the relative error between $\Delta E(x, y)$ and $E_{\text{ref}}(x, y)$ over the sampling grid using the 1-norm, which shows a prediction accuracy of over 92%.

B. Patch Antenna Array

In the section, the efficiency and accuracy of the proposed method is to be examined by resorting to measurement on a realistic antenna array operated at GHz frequencies. To minimize measurement interference, a miniaturized H-field probe with a 3.1 mm tip diameter is used for near-field scanning. A picture of the measurement setup is shown in Fig. 6(a). The antenna array is excited with a continuous 3 GHz signal, below its operating frequency of 5 GHz, to prevent unintended reflections from the industrial robotic arm during the OTF scan [16], [17]. The antenna array measures 20 cm×20 cm and comprises eight patch antennas connected through a cascaded phase-shifting network using microstrip lines. To accommodate the robot's kinematics, all rapid near-field OTF scans are optimally conducted along the y-axis, perpendicular to the array's feeding line.

For reference, the y-component of the H-fields, $H_{\text{ref}}(x, y)$, is first measured using up to 301 row scans over a 30 cm×30 cm area, positioned 10 mm above the antenna array. Fig. 6(b) shows the resulting high-resolution H-field distribution, indicating strong reflections at the feed point at the bottom

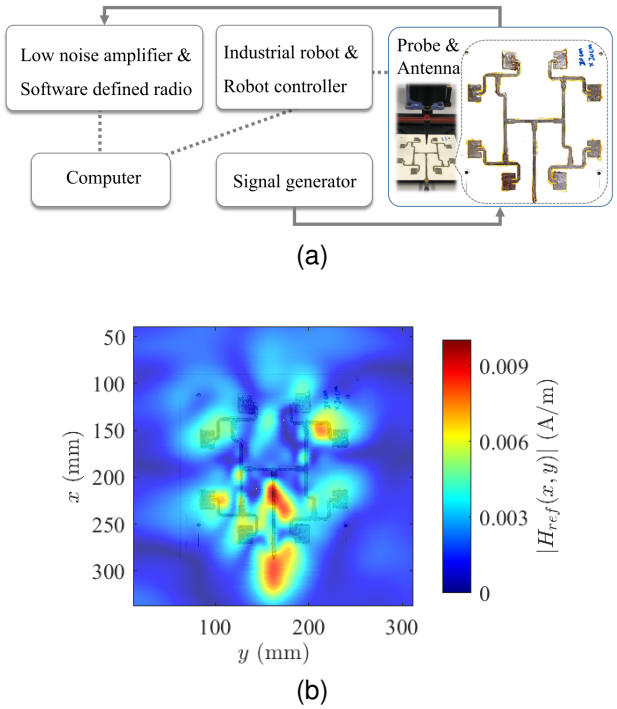

Fig. 6. Illustration of (a) the experimental setup using OTF scan [12], and (b) corresponding high-resolution H-field measurement (H_y only) at 3 GHz.

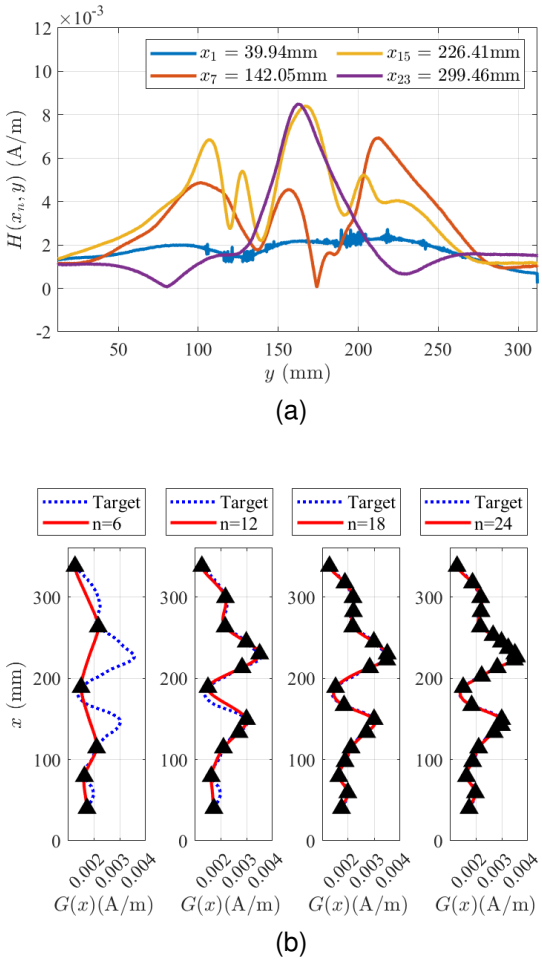

Fig. 7. Illustration of the adaptive OTF scan, showing (a) results of all row-wise scans, and (b) iterative predictions of $G(x)$ based on the first n scans.

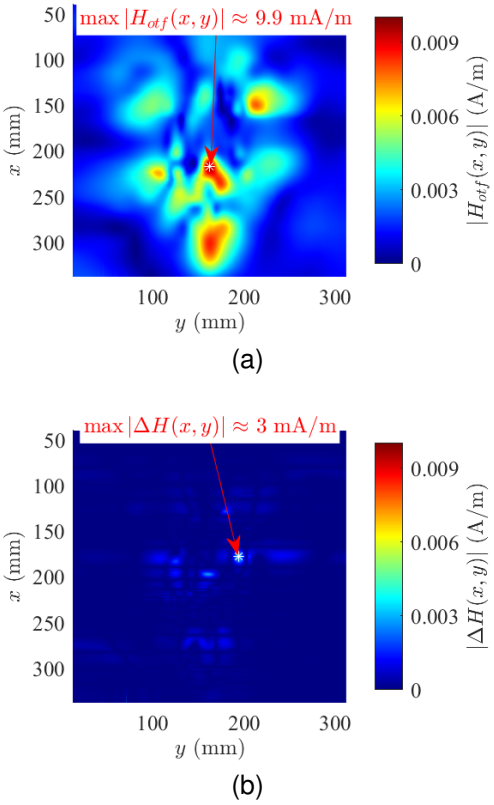

Fig. 8. Comparison of (a) H-field prediction obtained from adaptive OTF scan and (b) its deviation to the reference E-field results provided in Fig. 6(b).

and the first power divider in the middle due to impedance mismatches. The adaptive OTF scan is conducted, starting with five evenly spaced initial row scans. Meanwhile, the minimum number of OTF scans is set to 25 based on the numerical test in Fig. 5. After 20 additional row scans, the object function $G(x)$ is precisely captured, demonstrating the efficiency of the proposed adaptive scan method, as shown in Fig. 7. Similar to the simulation examples, the 2D near-field distribution, $H_{\text{otf}}(x, y)$, is visualized by interpolating the full grid based on all 25 row scans. Measurement accuracy is evaluated by calculating the deviation, $\Delta H(x, y)$, obtained by subtracting $H_{\text{otf}}(x, y)$ from $H_{\text{ref}}(x, y)$, as shown in Fig. 8. With a scanning speed of up to 2 m/s, each row scan takes approximately 1–2 seconds, resulting in a total scanning time of less than one minute for the adaptive OTF scan. This includes the time required for GPR-based BO, which is less than 0.1 second per iteration.

IV. Conclusion

This work introduces a novel adaptive sampling approach for planar near-field acquisition. Leveraging a state-of-the-art OTF scanning technique, the 2D planar sampling is simplified into a 1D curve-fitting process, effectively handled using the GPR based BO method. Numerical and experimental examples demonstrate the efficiency and reliability in managing near-fields with substantial complexity. Future research of the proposed method will explore its application in broadband scenarios for rapid near-field modeling and far-field prediction.

REFERENCES

[1] A. Yaghjian, "An overview of near-field antenna measurements," *IEEE Trans. Antennas Propag.*, vol. 34, no. 1, pp. 30–45, 1986.

[2] F. Ferrara, C. Gennarelli, and R. Guerriero, "Near-field antenna measurement techniques," in *Handbook of antenna technologies*. Springer, 2016, pp. 2107–2163.

[3] R. R. Alavi, R. Mirzavand, J. Doucette, and P. Mousavi, "An adaptive data acquisition and clustering technique to enhance the speed of spherical near-field antenna measurements," *IEEE Antennas Wireless Propag. Lett.*, vol. 18, no. 11, pp. 2325–2329, 2019.

[4] R. Rafiee Alavi, R. Mirzavand, A. Kiaee, and P. Mousavi, "An adaptive data acquisition technique to enhance the speed of near-field antenna measurement," *IEEE Trans. Antennas Propag.*, vol. 70, no. 7, pp. 5873–5883, 2022.

[5] Y. Zhang and L. Jiang, "A hybrid model-based data-driven framework for the electromagnetic near-field scanning," *IEEE Trans. Electromagn. Compat.*, pp. 1–10, 2024.

[6] Y.-R. Feng, L. Zhang, X.-C. Wei, and E.-P. Li, "Multi-frequency and multi-component sparse near field scanning based on active machine learning," *IEEE Antennas Wireless Propag. Lett.*, pp. 1–5, 2024.

[7] L. Zhang, Y.-R. Feng, B. Pu, X.-D. Cai, D. Li, X.-C. Wei, B. Mutnury, J. Fan, H. Chen, J. L. Drewniak, and E.-P. Li, "A novel machine-learning-based batch selection method in sparse near-field scanning," *IEEE Trans. Microw. Theory Techn.*, vol. 70, no. 11, pp. 5019–5028, 2022.

[8] S. Serpaud, A. Boyer, S. Ben-Dhia, and F. Coccetti, "Fast and accurate near-field measurement method using sequential spatial adaptive sampling (ssas) algorithm," *IEEE Trans. Electromagn. Compat.*, vol. 63, no. 3, pp. 858–869, 2021.

[9] S. Serpaud, A. Boyer, S. B. Dhia, and F. Coccetti, "Efficiency of sequential spatial adaptive sampling algorithm to accelerate multifrequency near-field scanning measurement," *IEEE Trans. Electromagn. Compat.*, vol. 64, no. 3, pp. 816–826, 2022.

[10] J. Mangum, D. Emerson, and E. Greisen, "The on the fly imaging technique," *Astronomy & Astrophysics*, vol. 474, no. 2, pp. 679–687, 2007.

[11] C. Yang, C. Adam, and S. Götschel, "Single-probe near-field phase retrieval using on-the-fly scan and hilbert transform," in *2023 International Symposium on Electromagnetic Compatibility – EMC Europe*, 2023, pp. 1–6.

[12] ——, "Evaluation of on-the-fly scanning effects on complex field retrieval using a single probe," in *2024 International Symposium on Electromagnetic Compatibility – EMC Europe*, 2024, pp. 317–322.

[13] ——, "Complex near-field measurement using on-the-fly scan with in-phase and quadrature demodulation," in *2024 15th German Microwave Conference (GeMiC)*, 2024, pp. 181–184.

[14] P. I. Frazier, "A tutorial on bayesian optimization," 2018. [Online]. Available: https://arxiv.org/abs/1807.02811

[15] CONCEPT–II. Institut für Theoretische Elektrotechnik. Hamburg, Germany. [Online]. Available: https://www.tet.tuhh.de/concept-ii-familie/

[16] VS-6577, six-axis industrial robot. DENSO WAVE INCORPORATED. Aichi, Japan. [Online]. Available: https://www.denso-wave.com/

[17] EM-ISight, electromagnetic scanning system. APREL. Ontario, Canada. [Online]. Available: https://www.aprel.com/em-isight/